Morphology, Microstructure, and Rheology of Amphiphilic Telechelics Incorporating Polyhedral Oligosilsesquioxane

Byoung-Suhk Kim[†] and Patrick T. Mather[†,‡,§,*]

Polymer Program and Department of Chemical Engineering, Institute of Materials Science, University of Connecticut, Storrs, Connecticut 06269-3136, and Macromolecular Science and Engineering, Case Western Reserve University, Cleveland, Ohio 44106

Received September 6, 2006; Revised Manuscript Received September 24, 2006

ABSTRACT: Amphiphilic telechelics incorporating polyhedral oligosilsesquioxane (POSS) end-caps were synthesized and studied as a novel building block for the construction of inorganic−organic hybrid materials. Their micron-scale morphologies were investigated using hot-stage polarizing optical microscopy (POM), revealing a dramatic influence of POSS macromer incorporation. The molecular-scale crystalline microstructures of amphiphilic POSS telechelics were investigated using wide-angle X-ray diffraction (WAXD), revealing significant crystallinity for both POSS-rich and PEO-rich microdomains. This observation clearly indicates that distinct microstructures form from the covalently linked POSS endcaps and PEO bridges. Covalent endcapping by POSS macromers also disrupts the crystallization of PEO for particular compositions, resulting in less ordered PEO crystallites. Further evidence for microphase separation is given by rheological experiments on a selected amphiphilic POSS10k telechelic (**Tel10k**) that shows evidence for an order−disorder transition (ODT) akin to block-copolymer behavior. We conclude that POSS moieties, attached to both ends of PEG, aggregate and crystallize as nanocrystals.

Introduction

The self-assembly behavior of block copolymers and of hydrophobically modified polymers has been extensively studied as a building block approach to the processing of nanostructured materials at the molecular scale. Various block copolymers have been of scientific interest because they exhibit a wealth of microphase structures and have served as model systems for the study of phase transitions, owing to their slow molecular dynamics and control over molecular weight.[1−3] Recently, organic−inorganic nanocomposites have attracted a great deal of attention based on early findings of enhanced thermal and mechanical properties.[4,5] Hybrid materials in the form of copolymers based on inorganic and organic comonomers may display enhanced properties by bridging the property space between two dissimilar types of materials to give rise to a nanoscaled inorganic phase bound to an organic phase with controlled domain size via reduced interfacial tension between phases. Along these lines, polyhedral oligosilsesquioxane (POSS) materials are attractive candidates for designing hybrid materials at the molecular level; i.e., a 'bottom-up' approach.

Most research concerning POSS-containing polymers has focused on altering thermomechanical properties and thermo-oxidative stability both in thermoplastic[6−9] and thermosets.[10−12] Recently, Coughlin et al.[13,14] reported that in copolymers formed between ethylene and POSS-containing macromonomers, the pendent POSS units were found to aggregate and crystallize as nanocrystals. Hsiao et al.[15,16] reported that a unique class of polyurethane (PU) elastomers containing inorganic POSS molecules appears to form nanoscale crystals in the hard segment domains of PU and that the POSS molecules also enhance the microphase separation between the hard and soft segments. More recently Turri et al.[17] reported on ionomeric POSS polyurethanes utilizing poly(tetramethylene glycol) (PTMG) soft segments and both POSS diol and charged dimethylol propionic acid (DMPA) in the hard segments. They found that POSS incorporation up to a level of 10 wt-% allowed for the formation of aqueous dispersions and that the resulting materials featured crystalline POSS domains with unique surface properties. Due to the limited aggregation of POSS molecules to dimensions of 10−100 nm, the thermal and mechanical properties of POSS-containing polymers are expected to be improved over the parent polymer host. Such reinforcement may, in principle, arise either from isolated POSS units or from nanoaggregates of these units into larger POSS clusters. Clarification of the scale of reinforcement is an area of active pursuit in the field of POSS materials.

In our previous work,[18] we reported on the preparation of amphiphilic telechelics incorporating polyhedral oligosilsesquioxane (POSS), revealing that narrow and unimodal molecular weight distributions ($M_w/M_n < 1.1$) and close to 2.0 end-groups per PEG chain were achieved. Recently, we also reported capillary viscometry results showing that the associative behavior of the amphiphilic POSS telechelics in salt-free solution varies depending on the POSS content and the length of PEO block, affording a significant variation in hydrophobic/hydrophilic balance as well as solvent polarity.[19] Initial investigations have shown that these materials feature very unique properties in both solution and neat form. In addition to the modifications to bulk properties of PEO reported here, the large hydrophobic/hydrophilic contrast yields surface activity at the air/water interface.[20]

In the present work, we sought to investigate the microstructural and rheological characteristics of the synthesized amphiphilic POSS telechelics. We report the effect of POSS on crystallization behavior of PEO and microphase separation of PEO and POSS phases using polarized optical microscopy (POM) and differential scanning calorimetry (DSC). We also investigate the crystalline microstructures and rheological properties of the amphiphilic POSS telechelics by wide-angle

* Corresponding author. E-mail: patrick.mather@case.edu.
† Polymer Program, University of Connecticut.
‡ Department of Chemical Engineering, University of Connecticut.
§ Case Western Reserve University.

10.1021/ma062069i CCC: $33.50
Published on Web 11/18/2006

Table 1. Composition and Molecular Characteristic of the Amphiphilic POSS Telechelics

sample	MW of PEG ($\times 10^3$ g/mol)	[POSS]/ [PEG]	POSS (wt %)[a]	M_w/M_n[b]
Tel1k	1	2.15	68.1	1.02
Tel2k	2	2.16	52.7	1.08
Tel3.4k	3.4	2.03	40.7	1.02
Tel8k	8	1.94	23.6	1.03
Tel10k	10	1.86	19.8	1.04

[a] Determined by ^{1}H NMR. [b] Molecular weight distribution obtained by GPC.

X-ray diffraction (WAXD) and rotational rheometry, respectively.

Experimental Section

Materials. Isocyanatopropyl dimethylsilycyclohexyl-POSS (POSS macromer) was provided by Air Force Research Lab, AFRL/PRSM, and used as received. Poly(ethylene glycol) (PEG) (molecular weight (MW) = 1k, 2k, 3.4k, 8k, and 10k g/mol, Aldrich) was purified by repeating twice the process of precipitation into *n*-hexane from chloroform solution. Amphiphilic POSS telechelics studied herein were synthesized by direct urethane linkage between the diol end groups of PEG homopolymers and the monoisocyanate group of POSS macromers as catalyzed by dibutyl tin dilaurate (DBTDL; Aldrich, 95% purity). The detailed synthesis and characterization are described in the previous report,[18] while the nomenclature, composition, and characterization of the obtained products are summarized in Table 1.

Measurements. The spherulitic or otherwise birefringent morphologies were analyzed using hot-stage polarized optical microscopy (POM). The samples used for crystallization analysis were sandwiched between two glass slides, first carefully and briefly melted on a custom controlled temperature hot plate around 200−250 °C, and subsequently cooled to room temperature, resulting in uniform films. The development of birefringent superstructure during or following crystallization was observed with an Olympus BX50 microscope equipped with crossed polarizers, a STC-200 hot stage from Instec Inc., and a composite color CCD camera (Panasonic GP−KR222). Images were acquired from the CCD camera at selected times and/or temperatures using a frame grabber and Linksys software (Linkam Scientific). Spatial dimensions were calibrated using a stage micrometer with 10 μm line spacing. Unless otherwise noted, a 20×/0.4 NA achromat long working-distance objective lens (Olympus LMPlanFI) was employed.

The thermal transitions of the samples were measured with a TA Instruments differential scanning calorimeter (DSC 2920) equipped with a mechanical intracooler (down to −60 °C) under a continuous nitrogen purge (50 mL/min). All measurements were conducted at a scan rate of 10 °C/min. Wide-angle X-ray diffraction (WAXD) experiments were performed at room temperature with powdered samples using a Bruker D5005 X-ray diffractometer operating at 40 kV and 40 mA. Nickel-filtered Cu Kα radiation was used for the measurements, along with an angular range of $5 < 2\theta < 50°$.

For linear viscoelastic measurements, the dynamic shear storage and loss modulus, $G'(\omega)$ and $G''(\omega)$, of the polymers were obtained from dynamic frequency sweeps using an ARES rheometer (TA Instruments, Inc.). Samples were compression molded as air-free disks. All measurements were carried out within the linear viscoelastic range, as confirmed by a lack of strain dependence of the dynamic storage modulus and loss modulus. Strain amplitudes, ranging from 0.01 to 0.1 were employed, all well within the linear viscoelastic regime of the materials investigated. The dynamic moduli were measured as a function of frequency, $0.1 < \omega < 100$ rad/s at various temperatures spanning $50 < T < 180$ °C for the **Tel10k**, and 55 to 80 °C for PEG10k homopolymer. The parallel plate geometry with plate diameters of 25 mm was used with sample thicknesses ranging from 0.9 to 1.0 mm.

Results and Discussion

Morphological Properties and Microphase Separation. The chemical structure of the amphiphilic POSS telechelic used is shown in Figure 1. Such telechelics are composed of poly(ethylene oxide) (PEO) as a hydrophilic part and POSS endcaps as a hydrophobic part. It was expected that the morphologies of such polymers would be determined by their unique molecular architectures. That is, while the hydrophilic and crystalline PEO segments have a tendency to form a crystalline structure, the hydrophobic and bulky POSS moieties may block PEO crystallization, due to the steric hindrance, possibly associating themselves to give the POSS aggregates via hydrophobic interactions. Therefore, the hydrophilic/hydrophobic balance will be an important key to control the morphologies as well as final microstructures of the amphiphilic POSS telechelics.

Polarized optical micrographs for the crystallized POSS telechelics are shown as they appeared at room temperature in Figure 2. While, in general, PEG homopolymers show spherulites with a 'Maltese cross' birefringence pattern[21] under crossed polarizers at room temperature (Figure 3(A), discussed below), **Tel10k** (POSS content = 19.8 wt %) and **Tel8k** (POSS content = 23.6 wt %) telechelics show irregular birefringence patterns, which have very fine microstructures (~1 μm), at room temperature. Such a change of the birefringence pattern (loss of Maltese cross) may be due to the presence of the bulky POSS units trapped within the interlamellar regions of PEO crystals, which may result in a significantly distorted (or random) orientation, in turn interrupting the prolonged radial growth associated with spherulites. **Tel3.4k** (POSS content = 40.7 wt %) shows peculiar birefringent patterns at room temperature, a temperature that we show later to be above the crystallization temperature for the PEO block upon cooling. We postulate, then, that this material exhibits *form* birefringence and behaves as a microphase-separated triblock copolymer with either a lamellar (most likely) or cylindrical mesophase. It is well established that the lamellar and cylindrical phases of block copolymers, by virtue of their subwavelength index-modulation, exhibit form birefringence that is relatively small in magnitude when compared to oriented polymers ($\Delta n_{orient} > 10^{-1}$ versus $\Delta n_{form} \sim 10^{-3}$).[22] Similarly, **Tel2k** (POSS content = 52.7 wt %) and **Tel1k** (POSS content = 68.1 wt %) also show some evidence of birefringence using POM, although these limited observations at a single temperature were unable to allow conclusion on the underlying microstructure. Therefore, we turned to variable-temperature (hot-stage) POM observations to further elucidate phase behavior of the materials.

Melting and crystallization behavior were investigated using polarizing optical microscopy on a custom controlled temperature hot stage. As shown in Figure 3, with increasing temperature, birefringence of both PEG10k homopolymer and **Tel10k** disappeared at 70 °C and the field appears black, indicating an absence of PEO crystalline entities. When the temperature was lowered again to a point below the melting point at a cooling rate of 10 °C/min, for some period of time the field remained black. Continued cooling led to the formation of fine bright (birefringent) spheres that appeared sporadically near $T = 40$ °C (for PEG10k) and which were interpreted to be sites where crystallization began. Finally, the spherulites impinge on each other and grow together, forming a densely packed array of polyhedra. In contrast to the **PEG10k** homopolymer, **Tel10k** undergoing the same thermal history displayed continuous formation of many new bright spots (crystal nuclei), probably due to a nucleating effect of the incorporated POSS macromers in the form of nanocrystals (discussed below). In addition, nuclei

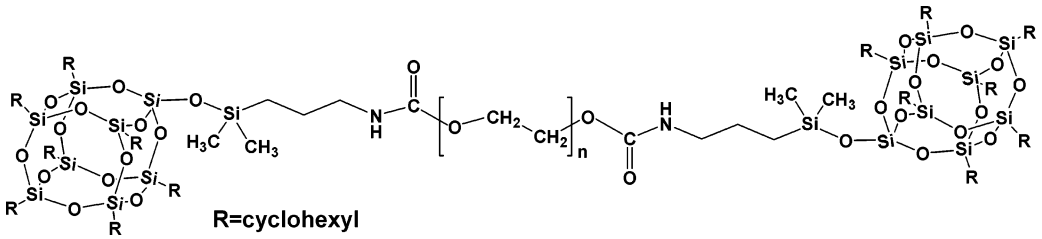

Figure 1. Chemical structure of the amphiphilic POSS telechelic.

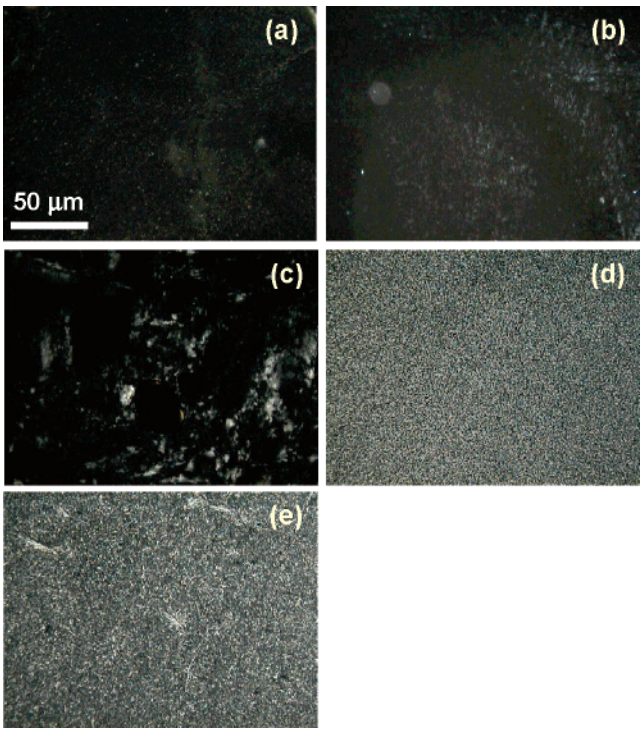

Figure 2. Polarized optical micrographs for the melt-cast films of the amphiphilic POSS telechelics at room temperature. (a) **Tel1k**, (b) **Tel2k**, (c) **Tel3.4k**, (d) **Tel8k**, and (e) **Tel10k**.

formation in **Tel10k** occurred at a lower temperature, $T_{cryst} \sim$ 20 °C, indicating significant crystallization suppression below that of the PEG10k homopolymer. Finally, we observed the complete absence of any Maltese cross pattern for **Tel10k**, suggesting that there is no coherent orientation pattern for the lamellar crystals forming the spherulites, probably due to a high nucleation density. Thus, the incorporated POSS end-groups, in the form of a higher-melting nanocrystalline phase, as we will show below in reference to Figures 5 and 7, play a significant role on both nucleation and growth of PEO crystallites during crystallization.

Figure 4 shows the polarized optical micrographs of the melt-cast amphiphilic POSS telechelic based on PEG3.4k (**Tel3.4k**) film at various temperatures. Specimens were sandwiched between two glass slides, first carefully melted until to flow on a custom controlled temperature hot stage around 200−250 °C and subsequently cooled to the lower temperature of −20 °C. When the temperature was increased at a heating rate of 10 °C/min, bright and strong birefringence attributed to the PEO crystalline phases and form birefringence started to disappear gradually, following which the field-of-view became dark at 25 °C, and indicating the melting of any crystalline entities of light-resolvable dimensions. These results also corresponded well with the melting point of crystalline PEO segments obtained by DSC.[18] Surprisingly, as the temperature was increased further, brightness between crossed polarizers reappeared around 28 °C, increasingly so with increasing temperature. This unusual finding was repeated several times and was quite reproducible. As this birefringent pattern persisted well beyond the melting temperature of PEO, we interpret the brightening as reaggregation of the POSS end-groups in the melted PEO matrix and associated form birefringence. The initial birefringence pattern recovers when the sample is cooled again to the lower temperature of −40 °C. In contrast, for the cases of **Tel8k** and **Tel10k** telechelics, as the temperature increases above the melting point of the PEO crystalline phases, the birefringence disappears quickly and then samples become completely dark under crossed polarizers. No evidence for form birefringence (attributed for **Tel3.4k** to the macroscopic separation of POSS crystal and PEO crystal phases) was found. However, as we show below for **Tel10k**, microphase separation is rheologically evident. We suggest, then, that the volume fractions of the POSS-rich phase in the **Tel8k** and **Tel10k** cases are small enough to result in a nonbirefringent block-copolymer phase (e.g., cubic spheres), unlike the case of **Tel3.4k**.

We also conducted DSC analysis in order to investigate the phase behavior of each POSS telechelic, as shown in Figure 5. We can see for these second heating DSC traces that increasing the POSS wt-% from sample **Tel10k** (19.8 wt-%) to **Tel1k** (68.1 wt-%) resulted in a clear decrease in both PEO-based T_m and ΔH_m and a simultaneous increase in POSS-based T_m. In our prior study, we observed the same systematic decrease in the melting temperature, T_m, and heat of fusion, ΔH_f, for the PEO-rich phase, with increasing POSS wt-%. Consistent with that study we show in Figure 5 complete suppression of PEO crystallization for the **Tel1k** and **Tel2k** telechelics. However, in that report we did not consider the phase behavior of the higher-melting POSS-rich phase. Inspection of Figure 5 reveals small and broad endothermic transitions in the temperature range 150 °C (onset) −210 °C for **Tel10k** and 220 °C (onset) − 260 °C for **Tel1k**. We note that the onset and peak temperatures for these transition, indicated as arrows in Figure 5, were determined using a scale more expanded than that shown.

In all cases, the high-temperature disordering (melting) endothermic transition was reversed on cooling in the form of an ordering (crystallizing) exothermic transition. For example, Figure 6 shows DSC thermograms of **Tel3.4k** that reveal its melting and crystallization behavior. In addition to complex melting of a PEO-rich phase, an additional endothermic peak was observed around 220 °C, due to POSS crystalline phase, and was reversible. These results correspond well with the results obtained by POM (Figure 4). The double melting transition in the $0 < T < 50$ °C region (Figure 6, heating traces), is attributed to the existence of PEO-based folded-chain lamellae with different fold numbers.[23]

Crystalline Microstructure. On the basis of our results from POM and DSC, we were motivated to more directly investigate the crystalline microstructure of the present POSS-containing polymers. In doing so, we hoped to gain understanding of the reinforcement mechanism of the higher mechanical and thermal

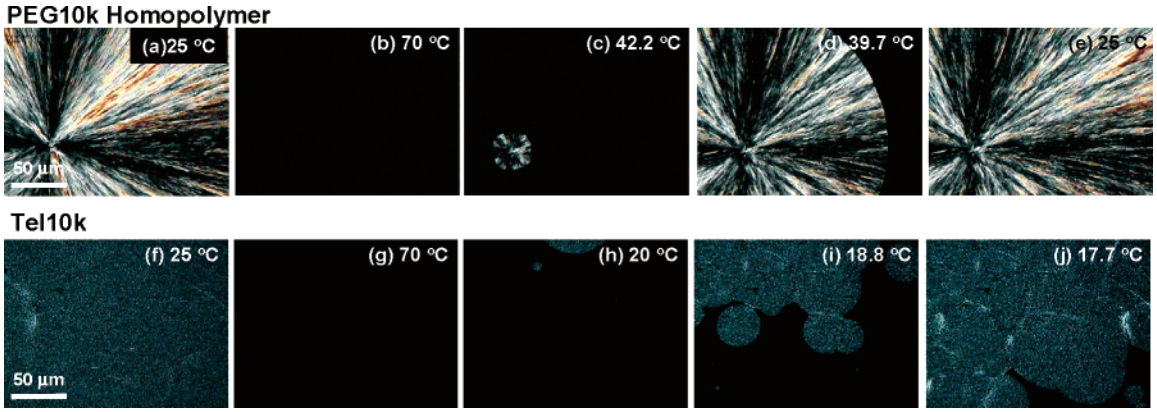

Figure 3. Observation of nucleation and spherulite growth by polarized optical microscope (POM) for the melt-cast (A) **PEG10k** homopolymer ((a) 25 °C, (b) 70 °C, (c) 42.2 °C, (d) 39.7 °C, (e) 25 °C) and (B) **Tel10k** ((f) 25 °C, (g) 70 °C, (h) 20 °C, (i) 18.8 °C, (j) 17.7 °C) at various temperatures. Heating and cooling rate was 10 °C/min.

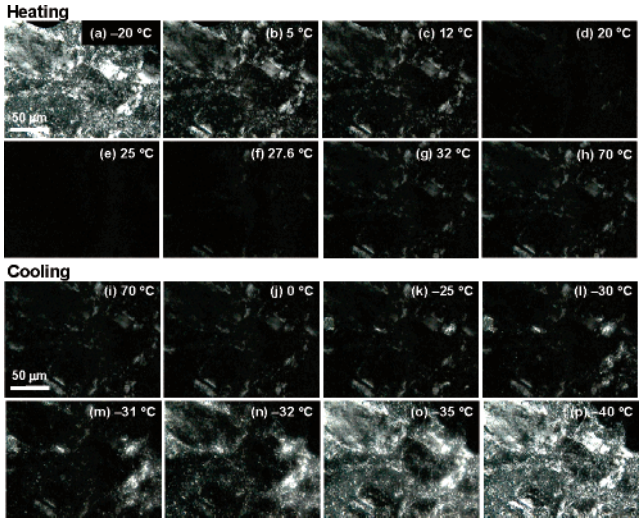

Figure 4. Polarized optical micrographs for the melt-cast films of **Tel3.4k** at various temperatures. (A) Heating cycle: (a) −20 °C, (b) 5 °C, (c) 12 °C, (d) 20 °C, (e) 25 °C, (f) 27.6 °C, (g) 32 °C, and (h) 70 °C. (B) Cooling cycle: (i) 70 °C, (j) 0 °C, (k) −25 °C, (l) −30 °C, (m) −31 °C, (n) −32 °C, (o) −35 °C, and (p) −40 °C. Heating and cooling rate were 10 °C/min and 5 °C/min, respectively.

properties. So far, such a reinforcement mechanism has been understood, in principle, by the hindered molecular motion due to the isolated POSS nanoparticle units[24,25] or the formation of the POSS aggregates[26,27] as a physical junction. Most previous research concerning POSS-containing polymers[24−31] has been focused on blends between the thermoplastic materials and POSS nanoparticles or the copolymerization using the POSS comonomers, resulting in a pendant POSS architecture. The present amphiphilic telechelic architecture, containing POSS macromers only at the chain ends, is unique and was therefore postulated to yield distinct properties. In particular, we anticipated that the combination of nearly monodisperse molecular weights and the configurational freedom of the POSS moieties as chain ends might allow for POSS crystallization ordinarily not observed in POSS copolymers.

Figure 7 shows the WAXD patterns at room temperature (T = 22 °C) of pure PEG homopolymer, synthesized amphiphilic POSS telechelics, and POSS macromer. **PEG8k** shows strong reflections at 2θ values of 19.1° (4.7 Å), 23.2° (3.8 Å), ∼27° (3.3Å), 36.2° (2.5 Å), and 39.6° (2.3 Å), corresponding to the PEO crystals in a helical conformation (monoclinic). The same reflections, and thus the same crystalline microstructure, were observed for amphiphilic POSS telechelics **Tel10k** and **Tel8k**.

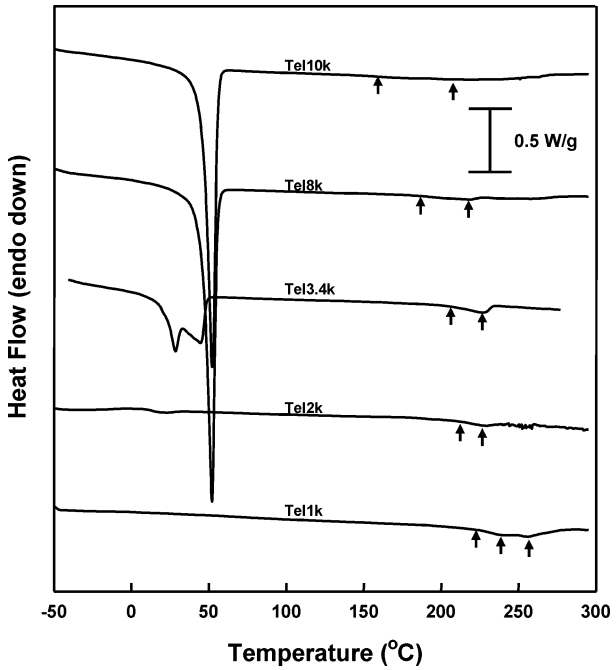

Figure 5. Differential scanning calorimetry (DSC) analysis of the POSS telechelics. Heating rate was 10 °C/min. Arrows indicate onset and maximum of higher temperature endothermic transition, determined on expanded scales.

The monoclinic lattice is commonly observed in PEO crystals, while the triclinic crystal featuring planar-zigzag chain conformations usually only seen under strong deformations.[32,33] Turning our attention to the lower angle regions of the scattering patterns, Figure 7 reveals that all crystalline peaks corresponding to the POSS moiety are preserved in the amphiphilic POSS telechelics, while those for PEO were preserved only in telechelics with sufficiently low POSS wt-%. Concerning the former, we clearly observed characteristic strong reflections at 2θ values of 7.8° (11.3 Å), 10.62° (8.3Å), and 18.20° (4.9 Å), all associated with a crystalline POSS phase. These strong reflections agree well with a rhombohedral unit cell with a = 11.57 Å and α = 95.5°, reported elsewhere for a POSS macromonomer with cyclohexyl corner groups.[16] Like Coughlin's polyethylene-POSS system,[13−14] the present materials represent a dual crystalline system wherein both POSS and PEO can crystallize, yet with competition. As the POSS content in the amphiphilic POSS telechelics was increased, three additional peaks from the POSS component become more apparent and sharp while the strong PEO reflections (d-spacings = 4.7, 3.8,

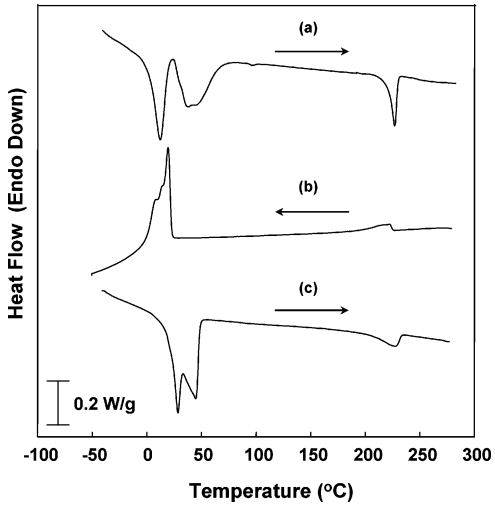

Figure 6. Differential scanning calorimetry (DSC) analysis of the **Tel3.4k**. (a) 1st heating curve, (b) 1st cooling curve, (c) 2nd heating curve. Heating or cooling rate was 10 °C/min.

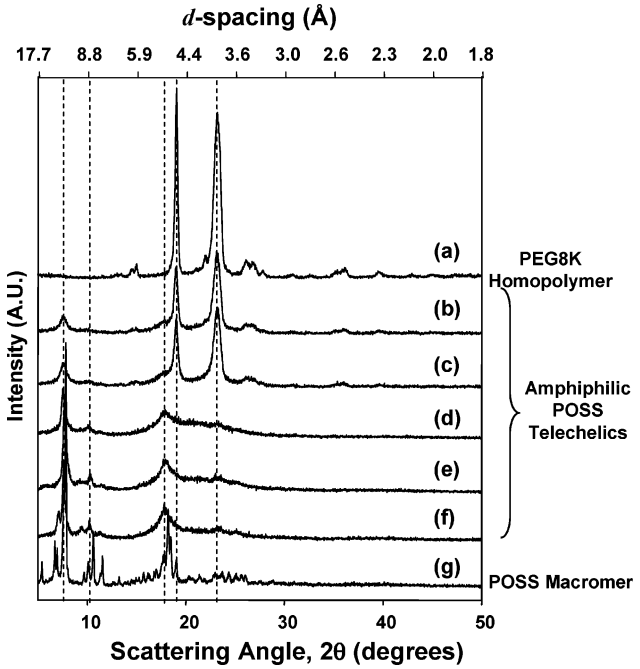

Figure 7. Wide-Angle X-ray diffraction (WAXD) patterns of the as-synthesized amphiphilic POSS telechelics. (a) **PEG8k**, (b) **Tel10k**, (c) **Tel8k**, (d) **Tel3.4k**, (e) **Tel2k**, (f) **Tel1k**, and (g) POSS macromer. Patterns are offset for clarity.

and 3.3 Å) were weakened to the point of disappearance, at least at room temperature.

These results suggest disturbance to PEO segment ordering[18] that results from a confining effect of an adjacent crystalline POSS phase on a crystallizing PEO phase. Such an issue has been well-studied for PS−PEO diblock copolymers where the glassy POSS block confines PEO crystallization to a degree that depends on phase geometry[34] and dimension.[35] Nevertheless, all prominent peak positions of PEO and POSS crystals in the amphiphilic POSS telechelics are almost identical to those of the pure PEG and POSS materials, indicating that the POSS aggregates have the similar microcrystalline structure to the POSS moiety and likewise for PEO. We expect that the energy penalty for incorporating a bulky POSS macromer into the PEO-rich phase prior to crystallization and thus into a PEO crystalline domain would be excessively high, given the strong hydrophobicity of POSS relative to PEO. Therefore, one would expect

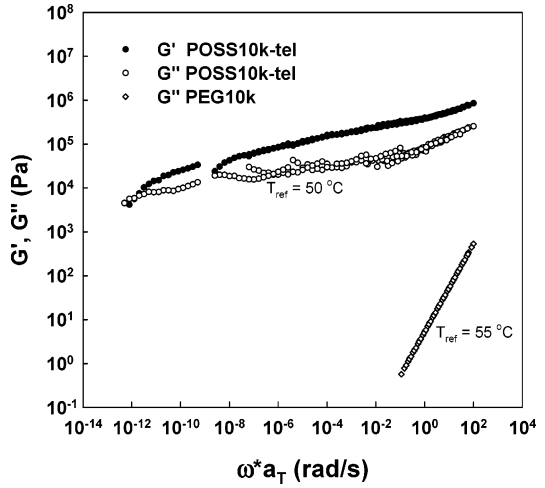

Figure 8. Dynamic modulus G′(ω) (filled circle) and G″(ω) (open circle) master curve for the **Tel10k** (ca. MW = 12k g/mol) (T_r = 50 °C) and G″(ω) (open diamond) master curve for the **PEG10k** (T_r = 55 °C).

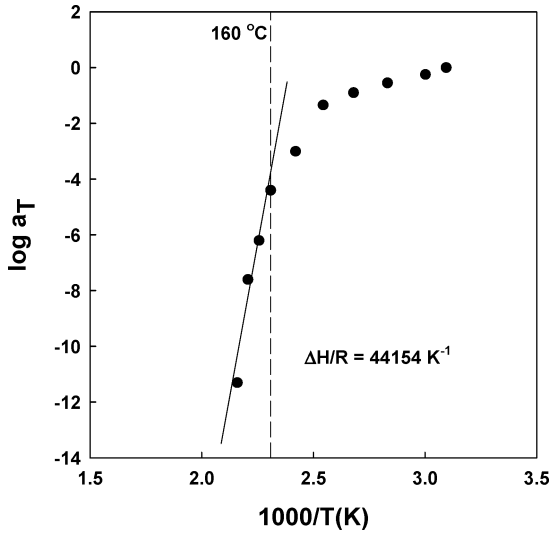

Figure 9. Shift factor, a_T, from the time−temperature superposition (TTS) for the **Tel10k**.

the incorporated POSS macromers to be preferentially excluded and separated from PEO crystallization. As a result, it was found that the amphiphilic POSS telechelics show microcrystalline features that are characteristic of the structures of the two separate components, that is, the dual system of PEO and POSS crystalline phases. Remaining, however, was identification of a microphase-separated state above the PEO T_m and POSS T_m, which we investigated with linear viscoelastic measurements.

Linear Viscoelasticity. The aggregation of the incorporated POSS end-groups may remarkably affect the rheological properties of the amphiphilic POSS telechelics compared to the pure PEG homopolymers. For instance, when the **PEG10k** homopolymer and **Tel10k** are heated thought the melting temperature of PEO crystalline segments, the **PEG10k** homopolymer becomes immediately molten, easily flowing, while **Tel10k** instead softens only to a rubbery state until melting above a temperature, $T \sim 180$ °C. Here, we describe this contrasting behavior quantitatively and explain the findings in light of our microscopy and thermal analysis results.

The dynamic shear moduli, within the linear viscoelastic regime, were characterized by frequency sweeps performed over a range of temperatures from 50 °C to 190 °C for **Tel10k** and from 55 °C to 80 °C for the parent **PEG10k** homopolymer.

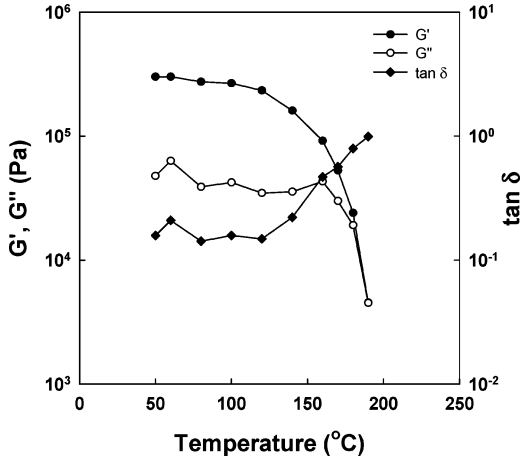

Figure 10. Temperature dependence of the dynamic storage and loss modulus (G' and G'') for the **Tel10k** upon cooling with $\omega = 0.1$ rad/s and stain amplitude = 0.03−0.04%.

Logarithmic plots of $G'(\omega)$ and $G''(\omega)$ taken at various temperatures were superimposed on those for reference temperature T_r by a translation of log a_T along the frequency axis. No shifts along the modulus axis were employed. Time−temperature superposition (TTS) can be expressed by:[26,36]

$$G^{\#}(\omega, T) = G^{\#}(\omega a_T, T_r) \quad (1)$$

where the symbol (#) stands for either one prime (′; storage) or two primes (″; loss). In this study, we chose reference temperatures T_r = 50 °C for **Tel10k** and T_r = 55 °C for the parent **PEG10k** homopolymer. As shown in Figure 8, we found that, above T_m^{PEO}, **PEG10k** features shear loss modulus (G'') values significantly greater than shear storage modulus G' values over the whole range of frequencies ($0.1 < \omega < 100$ rad/s), indicating that the system behaves as a liquid. In fact, we were unable to accurately measure $G'(\omega)$ for PEG10k using the conditions specified (particularly 25 mm diameter plates). On the other hand, we could easily measure the melt elasticity ($G'(\omega)$) above T_m^{PEO} for **Tel10k**, as G' values were at least several orders of magnitude higher than that of the **PEG10k** homopolymer.

In addition to the shear loss modulus spectrum for **PEG10k**, Figure 8 shows the master curves for both the storage and loss shear moduli of **Tel10k**. We found that this material fails to adequately obey time temperature superposition (TTS) for the range of temperatures explored. These results (which are quite reproducible) were not too surprising to us, given our findings on the underlying microstructure. In particular, the breakdown in time−temperature superposition that we observed suggests a secondary relaxation mechanism with distinct temperature dependence, which may be related to the rearrangement of POSS aggregates in the PEO matrix with changing temperature. Thus, these results are consistent with microphase separation in the **Tel10k** and, further, existence of phase change within the temperature range examined.

The storage modulus G' for **Tel10k** (possessing 20-wt % incorporation of the POSS macromer) is higher than G'' for nearly all temperatures and frequencies examined, indicating that, except at the highest temperature, **Tel10k** is rubbery, not relaxing stress via diffusion. The onset of a terminal zone (the lower frequency regime of fluidity) was only observed at the highest temperature examined, T = 180 °C. The overall increase in the dynamic shear moduli compared to the unmodified PEG10K homopolymer may be attributed to a resilient POSS-rich nanocrystalline phase, especially considering evaluation at much higher temperatures than the melting point of PEO crystalline phase. Furthermore, the previously discussed WAXD indicated that incorporated POSS macromers form nanocrystals, which apparently play a role of physical junctions in the PEO matrix system as indicated in the present rheological data.

Despite failure of TTS to allow construction of pristine master curves of the shear moduli for **Tel10k**, it is still meaningful to consider the shift factors employed in constructing Figure 8. When the shift factors, a_T, are plotted vs $1/T$ for **Tel10k** using an Arrhenius plot (Figure 9), a bilinear trend is observed with clear separation of low temperature and high-temperature behavior, beginning at T = 160 °C. The slope of the straight-line segment in the higher temperature regime (T > 160 °C) allowed calculation of an activation energy, E_a = 367 kJ/mol. This value is dramatically higher than activation energy measured for the un-modified **PEG10k** homopolymer (E_a = 31.9 kJ/mol, calculated based on the G'' curve) and even higher than the activation energy previously measured for POSS-containing polystyrene copolymers.[26] Given that the strong temperature-dependence of shift factors occurs in the same regime where fluidity begins to emerge, we postulate that the very high activation energy reflects the occurrence of a phase transition associated with the POSS-rich phase. To see this more clearly, we looked specifically at the temperature-dependence of the shear moduli.

Figure 10 shows the temperature-dependent rheological properties for **Tel10k**. For this experiment, the oscillation frequency and strain were 0.1 rad/s and 0.03−0.04%, respectively. All data were achieved after thermal equilibration at each temperature. For temperatures greater than T_m (ca. 63 °C) of the crystalline PEO segments, the POSS telechelic exhibits a high shear storage modulus of approximately 2×10^5 Pa. As a point of reference, this modulus is approximately 1 order of

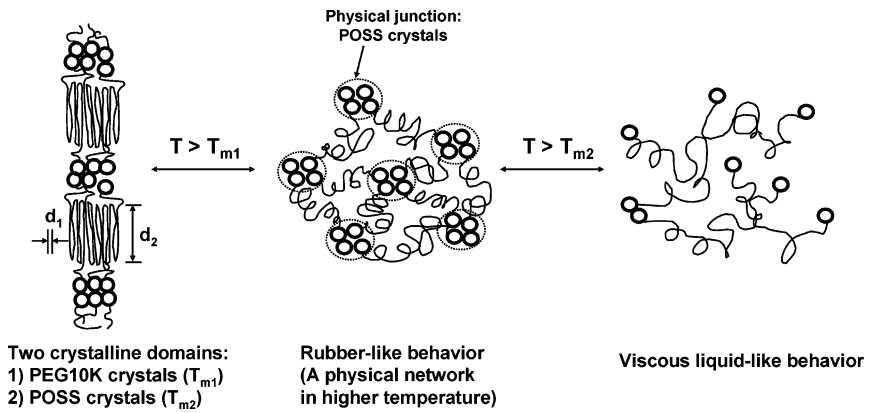

Figure 11. A proposed microstructure of **Tel10k** at various temperatures.

magnitude lower than the plateau modulus of entangled PEO (G_N^o = 1.8 MPa; M_e = 1800 g/mol).[37] As the temperature further increases, a precipitous drop in both G' and G'' occurs at 160 °C, the same temperature as the break observed in the Arrhenius plot of shift factors, suggesting the occurrence of an order−disorder transition (ODT) at that temperature. Without direct observations of temperature-dependent SAXS and WAXD, we can only postulate that this ODT transition is a complex combination of POSS melting and microphase homogenization. We further interpret the high-temperature rubbery modulus as originating from strong interactions between POSS macromers within ordered domains. We can calculate a molecular weight between physical cross-links to be M_c = 10,200 g/mol using the relation:

$$M_c = \frac{4\rho RT}{5G_N^{\,o}} \tag{2}$$

with a melt density estimate from ref 37 (1064 kg/m^3) and the modulus at 100 °C (2.6×10^5 Pa). As this value is larger than the 10 000 g/mol bridging group in the telechelics, we can infer that not all telechelic chains are elastically active and that the PEO is itself unentangled.

On the basis of light microscopy, thermal analysis, and rheology we conclude that, for temperatures below the POSS-based T_m, POSS exists in the form of a nanocrystalline phase. In particular, while Figure 3g shows no evidence of any crystals being present, Figures 5, 7, and 10 (DSC, WAXD, rheometry, respectively) all point to a crystalline POSS phase being present. Thus, we conclude that the crystals are too small to be detected optically and are therefore "nanocrystalline," with dimensions at least smaller than 800 nm. More generally, we draw in Figure 11 a schematic representation of POSS telechelic microstructure at various temperatures upon heating. At low temperature, both PEO (as folded lamellae) and POSS (as self-aggregates) crystalline phases coexist as a solid. Above the melting point of the PEO crystallites, the PEO crystalline phase disappears while POSS crystallites, acting as physical cross-linking sites, remain and preserve solid rheological character. Finally, as the temperature is risen above an order−disorder transition, the amphiphilic POSS telechelics becomes fluid.

Conclusions

Morphological, microstructural, and rheological properties of amphiphilic telechelics incorporating polyhedral oligosilsesquioxane (POSS) end-groups were investigated. We found that the morphologies of the PEO crystals were dramatically affected by POSS incorporation level and thus length of PEO block. The amphiphilic POSS telechelics showed irregular birefringence patterns under crossed polarizers, whereas unmodified PEG homopolymers revealed standard spherulites with 'Maltese cross' birefringence patterns. Such a change of the birefringence pattern upon POSS end-capping is argued to be due to a nucleating effect of a POSS nanocrystalline phase. This postulation was supported by DSC and WAXD analyses that revealed a higher temperature melting/crystallization temperature and crystalline POSS phase, respectively. Furthermore, some evidence for form birefringence above the PEO melting transition is reported. Amphiphilic POSS telechelics showed microstructural features characteristic structure of two separate crystalline components, that is, the dual system of PEO and POSS crystalline phases. The persistence of a POSS nanocrystalline phase at temperature between the melting transition of PEO and POSS led to dramatic alteration in physical properties, especially flow behavior. The dynamic moduli of the POSS10k-tel having about 20 wt % POSS content (**Tel10k**) was solidlike for a wide range of temperatures above the PEO melting temperature, but apparently underwent an order−disorder transition at a temperature near the apparent melting temperature for the POSS phase observed calorimetrically. Given this finding, along with clear evidence for microphase separation (DSC, POM, WAXD) of the telechelics into POSS and PEO domains, the amphiphilic POSS telechelics behave like triblock copolymers.

Acknowledgment. The authors thank Mr. Antonio Senador, Jr., for his assistance with the ARES rheometer experimentals. We gratefully acknowledge the support of AFOSR/NL through grant F49620-00-1-0100.

References and Notes

(1) Urich, R.; Chesne, A. D.; Templin, M.; Wiesner, U. *Adv. Mater.* **1999**, *11*, 141−146.
(2) Yu, K.; Zhang, L.; Eisenberg, A. *Langmuir* **1996**, *12*, 5980−5984.
(3) Muthukumar, M.; Ober, C. K.; Thomas, E. L. *Science* **1997**, *277*, 1225−1232.
(4) Haddad, T. S.; Lichtenhan, J. D. *Macromolecules* **1996**, *29*, 7302−7304.
(5) Laine, R. M.; Zhang, C.; Sellinger, A.; Viculis, L. *Appl. Organomet. Chem.* **1998**, *12*, 715−723.
(6) Xu, H.; Kuo, S.; Lee, J.; Chang. F. *Macromolecules* **2002**, *35*, 8788−8793.
(7) Haddad, T. S.; Viers, B. D.; Phillips, S. H. *J. Inorg. Organomet. Polym.* **2002**, 11(3), 155−164.
(8) Fu, B. X.; Gelfer, M. Y.; Hsiao, B. S.; Phillips, S.; Viers, B.; Blanski, R.; Ruth, P. *Polymer* **2003**, *44*, 1499−1506.
(9) Pyun, J.; Matyjaszewski, K.; Wu, J.; Kim, G. M.; Chun, S. B.; Mather, P. T. *Polymer* **2003**, *44*, 2739−2750.
(10) Abad, M. J.; Barral, L.; Fasce, D. P.; Williams, R. J. J. *Macromolecules* **2003**, *36*, 3128−3135.
(11) Choi, J.; Yee, A. F.; Laine, R. M. *Macromolecules* **2003**, *36*, 5666−5682.
(12) Kim, G. M.; Qin, H.; Fang, X.; Sun F. C.; Mather, P. T. *J. Polym. Sci., Part B: Polym. Phys.* **2003**, *41*, 3299−3313.
(13) Zheng, L.; Waddon, A. J.; Farris, R. J.; Coughlin, E. B. *Macromolecules* **2002**, *35*, 2375−2379.
(14) Waddon, A. J.; Zheng, L.; Farris, R. J.; Coughlin, E. B. *Nano Lett.* **2002**, *2*, 1149−1155.
(15) Fu, B. X.; Hsiao, B. S.; White, H.; Rafailovich, M.; Mather, P. T.; Jeon, H. G.; Phillips, S.; Lichtenhan, J.; Schwab, J. *Polym. Int.* **2000**, *49*, 437−440.
(16) Fu, B. X.; Hsiao, B. S.; Pagola, S.; Stephenes, P.; White, H.; Rafailovich, M.; Sokolov, J.; Mather, P. T.l Jeon, H. G.; Phillips, S.; Lichtenhan, J.; Schwab, J. *Polymer* **2001**, *42*, 599−611.
(17) Turri, S.; Levi, M. *Macromolecules* **2005**, *38*, 5569−5574.
(18) Kim, B. S.; Mather, P. T. *Macromolecules* **2002**, *35*, 8378−8384.
(19) Kim, B. S.; Mather, P. T. *Polymer* **2006**, 47, 6202−6207.
(20) (a) Lee, W.; Ni, S.; Kim, B. S.; Satija, S. K.; Mather, P. T.; Esker A. R. *Polym. Prepr. (Am. Chem. Soc., Div. Polym. Chem.)* **2006**, *47(2)*, 1214−1215. (b) Lee, W.; Ni, S.; Deng, J.; Kim, B. S.; Satija, S. K.; Mather, P. T.; Esker, A. R. *Macromolecules* **2006**, submitted.
(21) Schultz, J. M. *Polymer crystallization*; Oxford University Press: Oxford, 2001.
(22) (a) Folkes, M. J.; Keller, A. *Polymer* **1971**, 12, (4), 222−36. (b) Amundson, K.; Helfand, E.; Patel, S. S.; Quan, X.; Smith, S. D. *Macromolecules* **1992** *25* 1935−1940. (c) Lee, H. H.; Jeong, W.-Y.; Kim, J. K.; Ihn, K. J.; Kornfield, J. A.; Wang, Z.-G.; Qi, S. *Macromolecules* **2002**, *35* 785−794.
(23) Bogdanov, B.; Vidts, A.; Van Den Bulke, A.; Verbeek, R.; Schacht, E. *Polymer* **1998**, *39*, 1559−1563.
(24) Lee, A.; Lichtenhan, J. D. *Macromolecules* **1998**, *31*, 4970−4974.
(25) Bharadwaj, R. K.; Berry, R. J.; Farmer, B. L. *Polymer* **2000**, *41*, 7209−7221.
(26) Romo-Uribe, A.; Mather, P. T.; Haddad, T. S.; Lichtenhan, J. D. *J. Polym. Sci., Part B: Polym. Phys.* **1998**, *36*, 1857−1872.
(27) Mather, P. T.; Jeon, H. G.; Romo-Uribe, A.; Haddad, T. S.; Lichtenhan, J. D. *Macromolecules* **1999**, *32*, 1194−1203.
(28) Mather, P. T.; Chun, S. B.; Matyjaszewski, K. *Polym. Prepr. (Am. Chem. Soc., Div. Polym. Chem.)* **2000**, *41* (1), 582−583.

(29) Zheng, L.; Farris, R. J.; Coughlin, E. B. *Macromolecules* **2001**, *34*, 8034−8039.
(30) Fu, B. X.; Xang, L.; Somani, R. H.; Zong, S. X.; Hsiao, B. S.; Phillips, S.; Blanski, R.; Ruth, P. *J. Polym. Sci., Part B: Polym. Phys.* **2001**, *39*, 2727−2739.
(31) Zhang, W.; Fu, B. X.; Schrag, E.; Hsiao, B.; Mather, P.; Yang, N.; Xu, D.; Ade, H.; Rafailovich, M.; Sokolov, J. *Macromolecules* **2002**, *35*, 8029−8038.
(32) Zhu, L.; Cheng, S. Z. D.; Calhoun, B. H.; Ge, Q.; Quirk, R. P.; Thomas, E. L.; Hsiao, E.; Yeh, F.; Lotz, B. *J. Am. Chem. Soc.* **2000**, *122*, 5957−5967.
(33) Takahashi, Y.; Tadokoro, H. *Macromolecules* **1973**, *6*, 672−675.
(34) Zhu, L.; Huang, P.; Chen, W. Y.; Ge, Q.; Quirk, R. P.; Cheng, S. Z. D.; Thomas, E. L.; Lotz, B.; Hsiao, B. S.; Yeh, F.; Liu, L. *Macromolecules* **2002**, *35*, 3553−3562.
(35) Huang, P.; Zhu, L.; Guo, Y.; Ge, Q.; Jing, A. J.; Chen, W. Y.; Quirk, R. P.; Cheng, S. Z. D.; Thomas, E. L.; Lotz, B.; Hsiao, B. S.; Avila-Orta, C. A.; Sics, I. *Macromolecules* **2004**, *37*, 3689−3698.
(36) Ferry, J. D. *Viscoelastic Properties of Polymers*, 3rd ed.; John Wiley & Sons: New York, 1980.
(37) Wu, S. *J. Polym. Sci., Polym. Phys. Ed.* **1989** *27*, 723−741.

MA062069I